https://doi.org/10.5194/amt-2022-282
Preprint. Discussion started: 14 October 2022

Atmospheric Measurement Techniques Discussions
Open Access

Long-term detection, mapping, and interpretation of the trend of ozone in China (1978-2020) by constructing long-term consistent ozone datasets

Rongqi Tang[1], Xiaodan Wu[1]*, Jingping Wang[1], Dujuan Ma[1], Qicheng Zeng[1], Jianguang Wen[2], Qing Xiao[2]

[1]College of Earth and Environmental Sciences, Lanzhou University, Lanzhou 730000, China

[2]State Key Laboratory of Remote Sensing Science, Aerospace Information Research Institute, Chinese Academy of Sciences, Beijing 100101, China

Correspondence: Xiaodan Wu (wuxd@lzu.edu.cn)

Abstract: The ozone distribution characteristics in the stratosphere or troposphere are worth to be clarified due to their positive/negative impact on climate and human health. Nevertheless, the vertical distribution characteristics of ozone in China have not been fully understood either due to the limited time period of individual satellite records or the inconsistency of the accuracy of ozone products between different satellite records. In response to this challenge, this study first identified the vertical sensitivity of AIRS in detecting trends and verified the sensitivity in the near ground using *in-situ* measurements. Moreover, these different satellite records were cross-validated in order to check their consistency. In order to construct long-term, consistent ozone datasets dating back to the 1970s was constructed by intercalibrating the ozone products of different satellites using the cumulative distribution function with consideration of the vertical sensitivity. The distribution of ozone in the stratosphere and troposphere was then identified at several altitude layers (i.e., 3 km, 5 km, 12 km, 26 km, 31 km, and 34 km) with obvious interannual variation. The results indicate the seasonal variation of ozone is more significant in the troposphere while the interannual variation of ozone is more significant in the stratosphere. The spatiotemporal variation of ozone in the stratosphere shows a strong dependence on altitudes, and opposite results can be found at different altitudes. The ozone in the troposphere does not present significant interannual variations but shows distinct regional distribution characteristics in the Qinghai Tibet Plateau and Inner Mongolia.

Key points: Troposphere and stratosphere; Ozone profile; Temporal and spatial distribution; Trend;

https://doi.org/10.5194/amt-2022-282
Preprint. Discussion started: 14 October 2022

1. Introduction

The content and distribution characteristics of ozone play an important role in the global ecological environment and human health (Konderite and Varotsos, 2002). Changes in stratospheric ozone will affect the earth-atmosphere system's radiant energy budget, and such an impact will extend to the climate (Fishman et al., 1979). For instance, the reduction of stratospheric ozone not only reduces the temperature of the stratosphere but also reduces the energy input to the troposphere, causing lower surface temperature (Ramanathan and Dickinson, 1979; Ramanathan and Feng, 2009). But on the other hand, it allows more solar long-wave radiation to pass through stratosphere and reach troposphere. Hence, the reduction of stratospheric ozone will compensate for the greenhouse radiative forcing, which is conducive in the context of global warming (Kondratyev and Varotsos, 1996). Compared to stratospheric ozone, the ozone in troposphere is a greenhouse gas because it has a strong absorption effect on 8-10 um infrared long-wave radiation (Andersen and Sarma, 2012). The large-scale increase of tropospheric ozone has become the most important environmental problem because it damages plant cell structure (Treshow, 1970) and reduces gross primary productivity (GPP) (Yue and Unger, 2014). Moreover, it brings great harm to human health since long-term exposure to ozone leads to increased mortality of cardiopulmonary diseases and respiratory diseases (Jerrett et al., 2009). Therefore, exploring the distribution characteristic of ozone in stratosphere and troposphere is essential within the framework of sustainable development.

There have been many studies dedicated to identifying the variation characteristics of ozone. Nevertheless, the total stratospheric ozone, the total tropospheric ozone, the near-surface ozone, and the total ozone were generally analyzed separately. For instance, Chen et al. (2014) found that the total ozone column volume in the Yangtze River Delta region dropped significantly from 1978 to 2013 based on TOMS and OMI data. Ball et al. (2018) indicated that ozone in the upper and middle stratosphere had recovered between 60N and 60S but the ozone in the lower stratosphere continued to decline. Consequently, total ozone column volume in the stratosphere showed no trend as the increase made up for part of the loss. Li (2020) pointed out that there is a rising trend of near-surface ozone in the west of China, but a slightly higher trend in the southwest of China and the edge of the Qinghai-Tibet Plateau. Due to the distinctive characteristics of ozone distribution in the vertical direction, the role of ozone in the atmosphere and the unique changes of ozone in troposphere and stratosphere were not fully understood, because previous studies focused on the total amount of ozone which encapsulates the changes in each layer and makes it impossible to understand the specific change process of ozone in different layers. In fact, the ozone in different layers

https://doi.org/10.5194/amt-2022-282
Preprint. Discussion started: 14 October 2022

are interrelated and interact on each other. For instance, the increase in tropospheric ozone may be caused by the infiltration of stratospheric ozone under certain climatic effects (Fishman et al., 1979; Wargan et al., 2018). And the ozone in the upper troposphere may become a source of ozone in the near-surface layer under the influence of climate. Moreover, the ozone at different altitudes may present opposite trends. Therefore, it is necessary to explore the spatiotemporal variation of ozone at different altitudes in order to figure out the amount and transmission mechanism of ozone in stratosphere and troposphere.

However, the identification of the spatiotemporal distribution of ozone is challenging, because different data sources and different calculation methods result in different findings. For instance, Li et al. (2019) analyzed the seasonal variation and spatial distribution characteristics of total ozone in China using 9 AERONET ground sites and the ozone column volume data of OMI. Ohyama et al. (2011) extracted the total tropospheric ozone column using Gosat's thermal infrared spectral radiation data. In order to retrieve the tropospheric ozone profile and expand the spatial range covered by TES (Tropospheric Emission Spectrometer) records, the ozone level 1B data of AIRS and OMI were combined. Due to the inconsistent length of time series and the differences in the datasets, they even draw opposite conclusions in some areas. Consequently, there is always a dispute over the variation of ozone at different altitudes since the derived trends of ozone in different studies are not comparable. Additionally, different lengths of data records generally result in the inconsistency of derived trends (Meier et al., 2007). Global Climate Observing System (GCOS) has emphasized the necessity of using at least 30 years' datasets to study the change of climate factors (Kilifarska, 2012).

Therefore, this study aims to explore the spatiotemporal variation of ozone at different altitudes with inter-consistent ozone datasets at the longest time series. For stratospheric ozone, more than 40 years of records were constructed by combining multi-sensor products (1978-2020), including SUBV, SBUV-2, and AIRS. The discrepancy between these datasets regarding their sensor characteristics as well as retrieval algorithms have been removed using the cumulative distribution function (CDF). While for tropospheric ozone, the longest AIRS records of nearly 20 years (2003-2020) were used. Based on these datasets, the spatial variation of ozone in different altitudes, the exchange of ozone between the stratosphere and the top of the troposphere, and the exchange of ozone at different heights of the troposphere were explored for the first time. This paper begins by describing the study area and experimental data (Section 2). Section 3 explains the analysis methods. Section 4 provides the results and discussion about the quality of the consistent dataset and the spatiotemporal distribution of ozone at different altitudes. Finally, Section 5 presents a

https://doi.org/10.5194/amt-2022-282
Preprint. Discussion started: 14 October 2022

brief conclusion.

2. Study area and experimental data

2.1 Study area

The transmission and accumulation of ozone are closely related to the terrain and climate. China is featured by complicated geomorphology, a great disparity in altitude, variety of climates, and change in vertical topography. Mountainous areas are numerous and widely distributed, accounting for 2/3 of the total area. The terrain presents a three-level gradual decline in altitude from west to east. Regarding climate types, the eastern and southern China have a monsoon climate; the northwest has a temperate continental climate, and the Qinghai-Tibet Plateau has a significant alpine climate. The monsoon climate is significant in China, with high temperature and rain in summer and cold and little rain in winter. But the continental climate is also strong in China. The northerly wind blowing from the mainland to the ocean prevails in winter, and the southerly wind blowing from the ocean to the land prevails in summer. The cold and dry winter monsoon occurs in the interior of Asia. Under this circumstance, most areas of China generally have less precipitation and temperature in winter, especially in the north. Such sunny and breezy weather is conducive to the production and accumulation of ozone (Huang et al., 2006). Furthermore, the complicated terrain in China breeds more diverse local climate types, which accelerates the flow of ozone (Wang et al., 2017a).

In addition to the natural factors, the rapid development of industrialization and urbanization are always accompanied by environmental problems, especially in areas where industry and agriculture are concentrated (Wang et al., 2017b). Because the development of industry and agriculture generally led to an increase in the content of man-made ozone precursors NOx and VOCs (Zhang et al., 2007; Huang et al.,2011). The east and central south China are large economic areas with high ozone precursor emissions, resulting in large near-surface ozone in eastern China. The near-ground ozone content has been monitored since 2012 in some cities of China, but many monitoring stations were built after 2015 in other cities with high levels of ozone (Silver et al., 2018; Yin et al., 2019). As shown in Fig. 1, the distribution of monitoring stations is uneven, which is concentrated in east China but sparse in west and northeast China. The short-term and sparse *in-situ* observations are insufficient to explore the spatiotemporal variation of ozone in the past decades. Satellite data provide important and efficient data sources for monitoring zone from a long-term and spatial continuity perspective. Therefore, the spatiotemporal variation of ozone at different altitudes was

https://doi.org/10.5194/amt-2022-282
Preprint. Discussion started: 14 October 2022

Atmospheric Measurement Techniques
Discussions

detected using satellite datasets. Given the various climate types and the unbalanced regional economy, the ozone distribution characteristics were investigated for different regions (i.e., Northeast, North, East, Northwest, Southwest, and Central South) of China (Fig. 1).

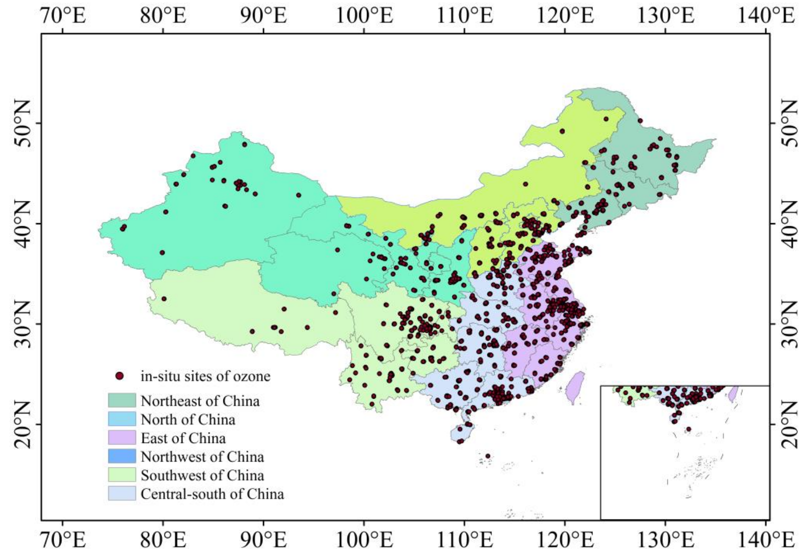

Fig. 1. Administrative zoning map of China and the distribution of ozone observation *in-situ* sites.

2.2 Experimental data

2.2.1 Satellite records

In order to monitor ozone from a long-term perspective, different satellite datasets, including SUBV Nimbus-7, SBUV-2 NOAA-11, SBUV-2 NOAA-16, and AIRS Aqua, were combined. The lifespan of different satellites is displayed in Fig.2. The whole period begins from September 1978 to December 2020. As seen from Fig. 2, there are always overlapping between different satellite-based observations, providing favorable conditions for the inter-calibration between these different satellite datasets.

https://doi.org/10.5194/amt-2022-282
Preprint. Discussion started: 14 October 2022

Atmospheric Measurement Techniques Discussions

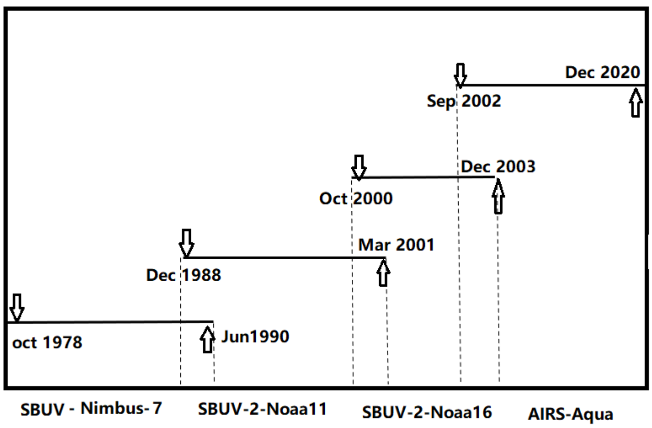

Fig. 2. The timespan of ozone datasets from different satellites used in this study.

The backward ultraviolet ozone vertical detector SBUV carried by Nimbus-7 was originally designed to measure stratospheric ozone. It covers the world every six days, with a total of 83 orbits, a spectral resolution of 1.1 nm, and a bandwidth of 3 nm. It observes the earth in a fixed nadir direction with an instantaneous field of view of 180 km × 180 km. NOAA V8 SBUV algorithm was used to generate ozone products. The wavelength channels used are 256, 273, 283, 288, 292, 298, 302, 306, 312, 318, 331, and 340 nm, respectively. Ultraviolet radiation of different wavelengths penetrates the atmosphere to provide information on ozone on different isobaric surfaces. The backward ultraviolet radiation at these 12 wavelengths is measured to obtain the total ozone and ozone vertical profile data.

The SBUV/2 carried by NOAA-11 and NOAA-16 is a further development of SBUV. Compared with the primary SBUV, it changes the band range and width of each UV channel. With its main working mode, the atmospheric backscattered solar radiation in near-ultraviolet light at 12 discrete wavelength bands was measured, ranging from 252.0 to 339.8 nm, with each bandpass of 1.1 nm. Considering that absorption should limit the penetration into the stratosphere, the wavelengths between 250 nm and 310 nm are used to retrieve the ozone profile products in SBUV-2. The V8.6 SBUV/2 algorithm uses a single-scattering forward iterative model to describe multiple scattering. It uses monthly cloud top pressure data, ice, and snow cover data with a spatial resolution of 1 degree to describe the effects of clouds, ice, and snow (Meijer et al., 2006), respectively. Priori ozone data and temperature profile data were used to constrain it in order to get the best estimate of ozone profile. Although the merger of SBUV and SBUV-2 ozone profile datasets have been conducted by many studies (Mcpeters et al., 2013; Frith et al., 2014; Ziemke et al., 2021), the merged products still suffer from considerable errors which has not been definitively explained. Moreover, the spatial resolution of the merged products is 5 degrees, which is too coarse to identify

https://doi.org/10.5194/amt-2022-282
Preprint. Discussion started: 14 October 2022

the distribution of ozone in China. Hence, the merged datasets were not adopted in this study. Instead, we construct the long-term dataset by inter-calibrating these different satellite datasets sequentially using the datasets over the overlapping period (Fig. 2). It is noteworthy that although there is a problem of orbital drift of NOAA_16, it occurred after 2004 which will not affect the inter-calibration using the cumulative distribution function (Fig. 2).

The AIRS mounted on Aqua satellite is a high spectral resolution atmospheric infrared detector with 2378 infrared channels. It is designed to work with two microwave sounders, including Advanced Microwave Sounding Unit-A (AMSU) and Humidity Sounder for Brazil (HSB), with a spatial resolution of 13.5 km. The main goal of scanning data is to observe the vertical structure of the earth's atmosphere. Since the start of operation in May 2002, the observation record of AIRS has continued to the present. AIRS has a high temporal resolution, scanning in the daytime ascending orbit and night descending orbit, covering more than 80% of the earth twice a day. The image is characterized by a large amount of overlap in high latitudes and gaps in parts of the equator. AIRS L2 inversion products include three inversion data source combinations, AIRS/AMSU/HSB, AIRS/AMSU, and AIRS-only. Due to the limited operation period of HSB and the decreased sensitivity of AMSU near the ground, the products produced by AIRS-only were selected in order to ensure the consistency of data products in time series. The V7 inversion algorithm does not use the two-regression method but instead the Stochastic Cloud Clearing/Neural Network (SCC/NN) (Evan Manning et al., 2020; Blackwell, 2012; Blackwell and Milstein, 2014; Tao et al., 2013) algorithm to generate an initial iterative value. Based on the initial state and a set of observed radiation values in the clear cloud state, the cloud-free coefficients can be generated to produce Initial clear column radiances. Based on the atmospheric infrared transmission equation, the physical problem can be solved using satellite observations, and then the final products can be generated. The temperature profile and ozone profile datasets were used in this study. The former refers to the absolute temperature while the latter indicates the mixing ratio of ozone. These two datasets provide 28 layers of data in the vertical direction.

2.2.2 In-situ data

Despite the short-term and sparse distribution of *in-situ* stations, *in-situ* measurements enable us to assess the performance of satellite ozone datasets. The *in-situ* ozone data is obtained from the national urban air quality real-time release platform, with the unit of ug/m^3 (microgram per cubic meter). There are 2024 monitoring sites, recording real-time ozone concentration each hour from 0:00 to 24:00. The *in-situ* ozone data is collected by a fixed ozone monitor installed on the top of urban buildings,

https://doi.org/10.5194/amt-2022-282
Preprint. Discussion started: 14 October 2022

Atmospheric Measurement Techniques Discussions

which represents the ozone concentration at a height of about 30 m above the ground. Since the overpass time of the Aqua satellite is 1:30 pm, the *in-situ* observations at 14:00 were extracted to match with satellite data. Considering data integrity and the consistency of temporal coverage of these *in-situ* sites, *in-situ* observations extending from January 1, 2017, to December 31, 2020, were picked out for evaluating the performance of AIRS ozone at 1000 hp.

3. Methodology

3.1 Quality assessment

3.1.1 The evaluation of AIRS ozone dataset

The direct comparison between *in-situ* and satellite-based measurements is generally conducted to assess the performance of the latter (Cazorla et al., 2021; Hulswar et al., 2021). Here, it was adopted to assess the performance of AIRS ozone dataset. Firstly, we convolve the average kernel provided by AIRS level-2 products with the *in-situ* data to reduce the observation difference. Then the AIRS pixel which is closest to *in-situ* site was extracted to match with *in-situ* measurements. Particularly, if there was more than one *in situ* site located within one AIRS pixel, the measurements of these sites were averaged to get only one ground-based value for comparison with AIRS measurements. Several indexes including root mean square error (RMSE) and correlation coefficient (R) were selected to measure the accuracy of AIRS ozone profile products near the ground. The former is used to describe the average deviation between the two datasets while the latter is used to measure their consistency.

$$RMSE = \sqrt{\sum_{i=1}^{n} (A_i - S_i)^2 / n} \quad (1)$$

$$R = (A_i - \bar{A})(S_i - \bar{S}) / \sqrt{\sum_{i=1}^{n} (A_i - \bar{A})^2 \sum_{i=1}^{n} (S_i - \bar{S})^2} \quad (2)$$

Where A_i is the AIRS pixel value, S_i represents the in-situ reference value matched to the satellite pixel, n indicates the total number of samples matched, $\bar{A}$ and $\bar{S}$ denote the averaged value of the AIRS data and in-situ data, respectively.

It is important to note that the direct validation results may contain uncertainties and should be interpreted with caution. This is partly because there is large spatial scale mismatch between in situ and satellite-based measurements, and partly because the measurement height between *in situ* and satellite measurements are not consistent. The

https://doi.org/10.5194/amt-2022-282
Preprint. Discussion started: 14 October 2022

Atmospheric Measurement Techniques
Discussions

zone measured by AIRS is at 1000 hp (i.e., ~110 m) while the height of in situ measurements ranges from 20 m and 30 m (MEPC, 2013). In order to reduce the impact of these factors on results, the data points with absolute differences larger than 20 ug/m^3 were excluded from the analysis.

3.1.2 Cross-comparison between different satellite datasets

In order to investigate the consistency between different satellite datasets, these four satellite products were compared during their overlapping periods (Fig. 2). In order to achieve a perfect spatial scale match between these different satellite datasets, all products were re-projected on a geographic grid of 0.6-degree squares. Considering the fact that the stratospheric ozone are relative stable during a short time period, all these satellite datasets were temporally aggregated to the monthly scale partly to elimite the discrepancy of the temporal resolution between different satellite datasets and partly to remove the outliers due to high-frequency processes such as wind blowing and other disturbances. The cross-comparison was carried out between each pair of ozone products at the heights of 26 km, 31 km, and 34 km. These heights were selected because they display relatively large interannual variations (Fig. 7) and the consistency between these satellite datasets plays a critical role in detecting the spatiotemporal variation of ozone from a long-term perspective. The consistency and closeness between these products were measured by RMSE and R.

3.2 The construction of long time series Ozone (1978-2020)

Here, the cumulative distribution function (CDF) was employed to eliminate the discrepancy between each pair of these satellite datasets. It has been applied to match soil moisture data (Liu et al., 2011), land surface emissivity (Zhang et al., 2018), and chlorophyll fluorescence (Wang et al., 2021), and has been proved to be able to improve the relative accuracy of different satellite datasets without involving complex physical mechanisms and damaging the trend in time series. CDF is the integral of the probability density function. The high-order polynomial was used to match the cumulative distribution functions of two datasets during the overlapping period. Then the two datasets can have the closest cumulative probability distribution. In this way, the goal of creating an inter-consistent ozone dataset in long time series can be achieved. The specific description is as follows:

$$F(x) = Pr(X \le x) \quad -\infty \le x \le +\infty \tag{3}$$

where $F(x)$ is the cumulative distribution function, X denotes the value of the sample, and $Pr(X \le x)$ represents the probability that the sample value is less than a certain

https://doi.org/10.5194/amt-2022-282
Preprint. Discussion started: 14 October 2022

value of x. In order to match the CDF between different products, the fitting function is required:

$$\mathrm{F(x)} \approx f(x, x^2 \ldots x^n) \tag{4}$$

where $f(x, x^2 \ldots x^n)$ represents the nth degree polynomial about the independent variable x, which is used to fit the CDF of each satellite product.

In this study, AIRS dataset was used as the benchmark during the CDF matching partly because of its good performance in detecting trends in the stratosphere and troposphere (Rawat et al., 2022, Bian et al., 2007, Wang et al., 2019, Maddy et al., 2008) and partly because it offers the longest time serial data (Fig. 2). SBUV-2 ozone profile dataset was matched to AIRS on the pixel basis during the overlapping period. The calibration coefficients were calculated per pixel and then applied to the SBUV-2 dataset over its whole time series. Similarly, the matching procedure was conducted for each pair of satellite datasets from back to front during their overlapping period. In this way, a consistent ozone dataset was generated dating back to the 1970s.

3.3 Spatiotemporal distribution characteristics identification at different altitudes

The spatial distribution of ozone was explored by calculating the multiyear annual averaged ozone on the pixel basis. Furthermore, the standard deviation of the annually averaged ozone was calculated on the pixel basis to show the degree of interannual fluctuations over different areas. Regarding the trend of ozone, the least-squares-based linear fitting method, in which time is the independent variable and the ozone mixing ratio is the dependent variable, was applied. Additionally, the significance of the interannual trend was tested using t-test, and the significant trends ($p<0.05$) were retained. In order to explore whether the interannual variation of ozone in China was dominates by the change of ozone in the individual month, the interannual trends were also calculated for each month. Moreover, in order to display the difference of ozone between different layers more intuitively, a simple empirical formula was adopted to convert atmospheric pressure into altitude:

$$H_s = (R/M_r g) \cdot T_m \cdot \ln\left(\frac{P_0}{P_S}\right) \tag{5}$$

where R is the ideal gas constant, g is the gravitational acceleration, T_m is the reference temperature under the standard pressure, M_r is molar mass of air, and P_0 is the ground standard pressure. They were set as 8.31 $\mathrm{J} \cdot mol^{-1} \cdot K^{-1}$, 9.8 m/s^2, 300 K, 29 g/mol and 1013 pa, respectively. P_S represents the air pressure to be converted.

Although satellite datasets provide ozone at different altitudes, we only focused on several heights with relatively large temporal variations. Here, the ozone at the heights

https://doi.org/10.5194/amt-2022-282
Preprint. Discussion started: 14 October 2022

of 34 km, 31 km, and 26 km in the stratosphere and at the heights of 12 km, 5 km, and 3 km in the troposphere were focused. The former is based on fusion datasets from 1978 to 2020, while the latter is based on AIRS datasets from 2003 to 2020.

4. Result and discussions

4.1 Accuracy assessment

4.1.1 The evaluation of AIRS dataset based on *in-situ* sites

Given the fact that AIRS dataset was used as the benchmark during the CDF matching process, its ability to capture the gradient and variability of vertical ozone determines the quality of the long-term ozone data. Here, we present the direct comparison results between AIRS ozone and *in situ* ozone (2017-2020) (Fig. 3). In order to show whether the performance of satellite ozone dataset varies with time, we present the results for each year. It can be seen that the data points are distributed around line 1:1 over the four years. The AIRS and in situ-based ozone is generally in a good agreement given that the R between them is larger than 0.760 and RMSEs are smaller than 7.21 ug/m^3. Both the RMSE and R are relatively stable over the four years, demonstrating that the performance of AIRS dataset is basically stable. The former ranges from 6.05 ug/m^3 to 7.21 ug/m^3 and the latter ranges from 0.760 to 0.834.

https://doi.org/10.5194/amt-2022-282
Preprint. Discussion started: 14 October 2022

Atmospheric Measurement Techniques
Discussions

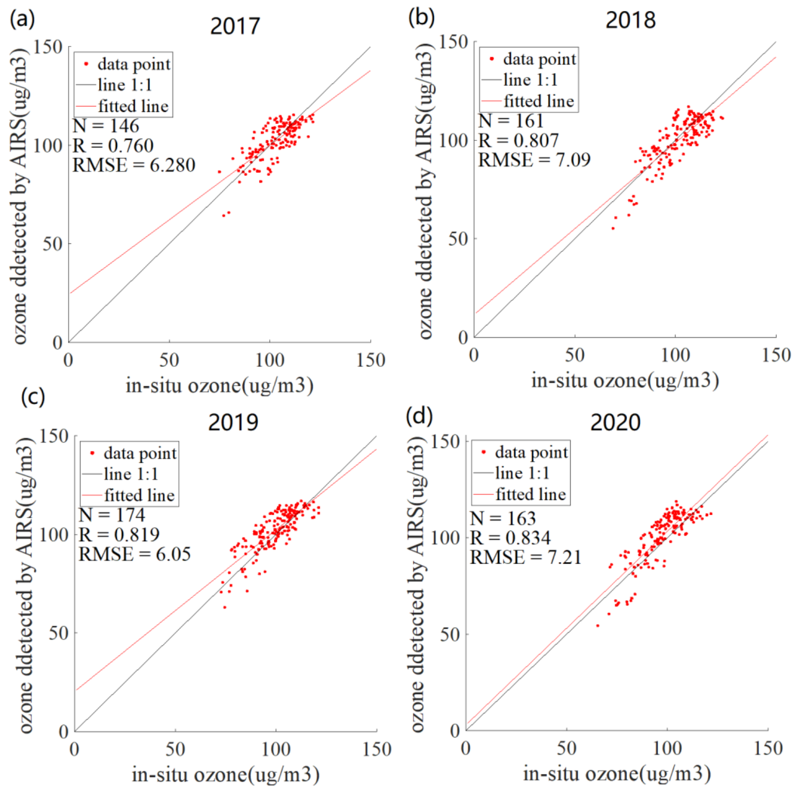

Fig. 3. The comparison of ozone between AIRS and *in-situ* measurements from 2017 to 2020.

It is noteworthy that since *in situ* site measured the ozone near the ground, the evaluation results can only indicate the performance of AIRS near the ground (~1000 hp). Although an independent validation of retrieved profiles at different levels is crucial for the correct use of satellite product, a comprehensive evaluation of the performance of AIRS ozone profile over such a vast area is too difficult to implement due to the lack of in situ ozone measurements at different levels of the retrieved profiles. In fact, such an evaluation can only be conducted over a specific area. For instance, Bian et al. (2007) conducted a direct comparison between AIRS and in situ measurements in Beijing and proved that AIRS could capture the distribution and change of ozone in the upper troposphere and lower stratosphere (UTLS). The good performance of AIRS in the range from 800 hp to 250 hp and those less than 50 hp has also been confirmed by Wang et al. (2019). Although AIRS present relatively large errors between 250 hp and 50 hp, it can capture the gradient and variability of ozone in the range from 250 hp to 50 hp well (Ma et al., 2019). Based on these studies, it is reasonable to consider that AIRS is able to capture the vertical gradient and variability of ozone in the stratosphere and middle and upper troposphere in China. Hence, it is

https://doi.org/10.5194/amt-2022-282
Preprint. Discussion started: 14 October 2022

safe to use AIRS ozone dataset as the benchmark to construct the long-term consistent ozone dataset.

4.1.2 Cross-validation

Fig. 4 present the cross-comparison results of each pair of datasets during their overlapping period. As for the results of Nimbus-7-SBUV vs. NOAA11-SBUV-2 (Fig. 4(a-c)), the best agreement appears at the height of 26 km, with the RMSE of 0.115 and R of 0.96. The consistency between them deteriorates at the height of 31 km, with R decreased to 0.746. But the RMSE is still very small with a value of 0.170 ppmv. As the height increased to 34 km, R increased to 0.88, but RMSE increased to 0.487 ppmv. The largest RMSE at the height of 34 km is partly attributed to their large deviations and partly attributed to the large ozone at this height. From Fig. 4(a-c), it can be found that the ozone at the height of 34 km is the largest among these three heights, with the values ranging from 5 to 8 ppmv. The height of 31 km follows, with the ozone ranging from 4 to 5. And the height of 26 km rank last, with the ozone ranging from 1.5 to 3. From Fig. 4 (d-f), it can be seen that the agreement between NOAA11-SBUV-2 and NOAA16-SBUV-2 are very good at the heights of 26 km and 31 km, with high R of 0.974 and 0.926, respectively. Furthermore, the RMSE between them is very small at the height of 26 km, with a value of 0.097 ppmv. But the RMSE increased to 0.189 ppmv when height changed from 26 km to 31 km. The larger RMSE is partly due to the significantly larger ozone at this height. Nevertheless, when the height increased to 34 km, their agreement is not so good, with R decreased to 0.643. But the RMSE is still reasonable, with the value of 0.241 ppmv. As for the cross-comparison results of NOAA16-SBUV-2 vs. AIRS (Fig. 4(g-i)), the consistency between them is still the best at the height of 26 km, with a high R of 0.973. But the RMSE is considerable, with the value of 0.211 ppmv. It is noteworthy that the consistency between them is not so good at the height of 31 km and 34 km, with R of 0.741 and 0.760, respectively.

From the above results, it can be seen that the cross-comparison results show high dependence on the pair of satellite datasets and the height. Generally speaking, the consistency between NOAA11-SBUV-2 and NOAA16-SBUV-2 is the best among these three pairs. The consistency between Nimbus-7-SBUV and NOAA11-SBUV-2 follows. And that of NOAA16-SBUV-2 vs. AIRS rank last. Regarding the influence of height, the best agreement occurs at the height of 26 km. But the results of 31 km and 34 km is unstable and show dependence on pair of satellite datasets

https://doi.org/10.5194/amt-2022-282
Preprint. Discussion started: 14 October 2022

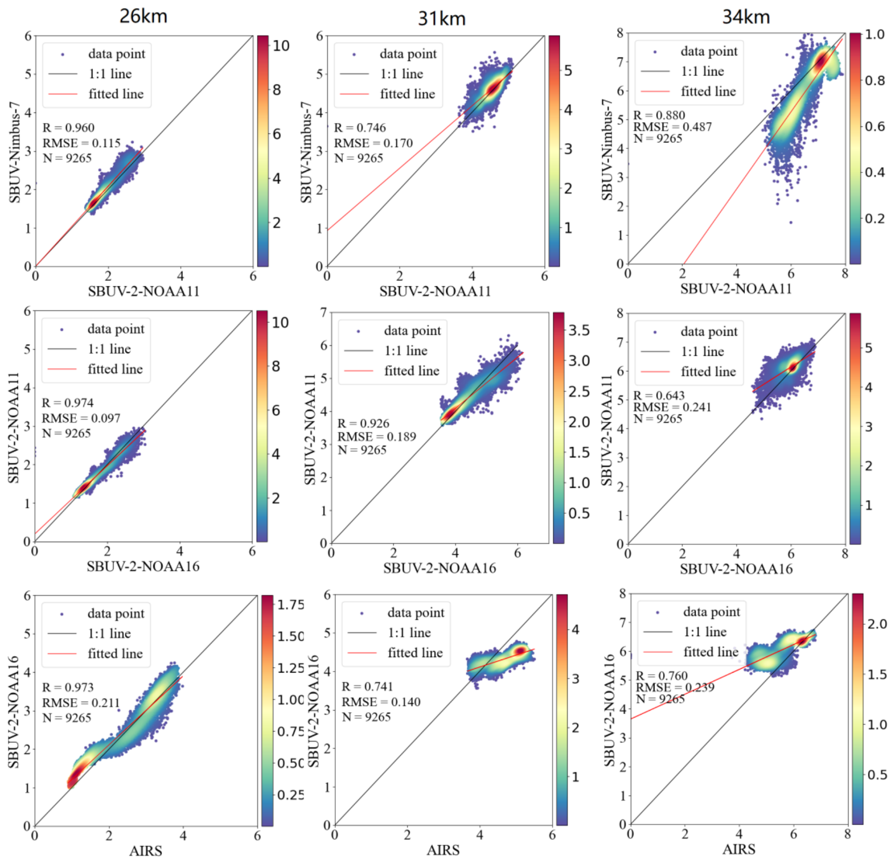

Fig. 4. The cross-validation results between theses satellite datasets at three heights during their overlapping periods: the first to third columns indicate the results at 26 km, 31 km, and 34 km, respectively. The first to third rows indicate the comparison results of Nimbus-7-SBUV vs. NOAA11-SBUV-2, NOAA11-SBUV-2 vs. NOAA16-SBUV-2, and NOAA16-SBUV-2 vs. AIRS, respectively.

4.2 Inter-calibration by CDF

The pixel-based CDF match was conducted between Nimbus-7-SBUV and NOAA11-SBUV-2, NOAA11-SBUV-2 and NOAA16-SBUV-2, and NOAA16-SBUV-2 and AIRS, respectively. Here, only the results of NOAA16-SBUV-2 vs. AIRS are shown for conciseness (Fig. 5). It can be seen that their cumulative distribution curves below 3 ppmv match quite well when ozone is less than 3.5 ppmv, but large deviation can be observed when ozone is larger than 3.5 ppmv. Given the fact that AIRS has the longest time series and has been evaluated with *in situ*-based measurements, it functions

https://doi.org/10.5194/amt-2022-282
Preprint. Discussion started: 14 October 2022

Atmospheric Measurement Techniques Discussions

as the reference to calibrate the NOAA16-SBUV-2 with CDF matching. It can be seen that the cumulative distribution function of the calibrated NOAA16-SBUV-2 agree well with that of AIRS, indicating that the discrepancy of ozone between these two satellite products has been corrected. Then the calibrated NOAA16-SBUV-2 is used as the reference to calibrate NOAA11-SBUV-2. Similarly, the Nimbus-7-SBUV was calibrated with the calibrated NOAA11-SBUV-2.

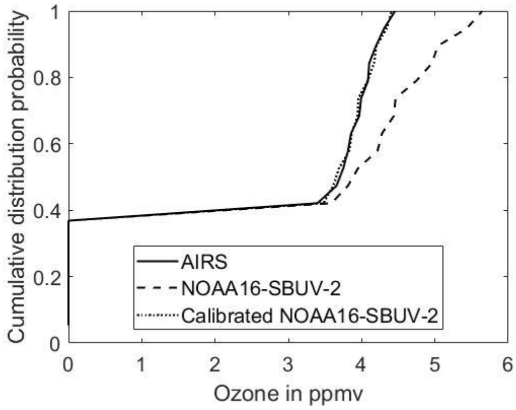

Fig. 5. A typical cumulative distribution function between AIRS and SBUV-2 at the height of 34 km before and after the CDF match.

Fig. 6 presents the scatterplots between different datasets after CDF matching. The performance of CDF matching can be further evaluated by comparing the improvement of the agreement between different calibrated satellite datasets to those without CDF matching (i.e., Fig. 6 vs. Fig. 4). There is always an improvement of the agreement between Nimbus-7-SBUV and NOAA11-SBUV-2 at different heights (Fig. 6(a-c)). R increased from 0.96, 0.746, and 0.88 to 0.983, 0.803, and 0.938 at the height of 26 km, 31 km, and 34 km, respectively. There is no obvious change of RMSE at the height of 26 km (0.108 vs. 0.106) and 31 km (0.140 vs. 0.157). But RMSE decreased significantly from 0.487 ppmv to 0.236 ppmv at the height of 34 km. By contrast, there is no obvious improvement of the agreement between calibrated NOAA11-SBUV-2 and calibrated NOAA16-SBUV-2 (Fig. 6(d-f)). There is no improvement of R and RMSE at the height of 26 km and 31 km. But a slight improvement appears at the height of 34 km, with the R increased from 0.643 to 0.757 but RMSE increased from 0.241 ppmv to 0.472 ppmv. This phenomenon is partly related to the fact that their overlapping period is so short (Fig. 2) that the data points used for CDF matching are very limited. Regarding the agreement between calibrated NOAA16-SBUV-2 and AIRS (Fig. 6(g-i)), there is significant improvement at the height of 31 km and 34 km, with R increased from 0.741 and 0.760 to 0.851 and 0.879, respectively. And the RMSEs decreased from 0.140 ppmv and0.239ppmv to 0.0.125 ppmv and 0.228 ppmv, respectively. Nevertheless, the

https://doi.org/10.5194/amt-2022-282
Preprint. Discussion started: 14 October 2022

Atmospheric Measurement Techniques
Discussions

agreement between them even deteriorates at the height of 26 km. RMSE decreased from 0.211 ppmv to 0.16 ppmv but R decreased from 0.973 to 0.952.

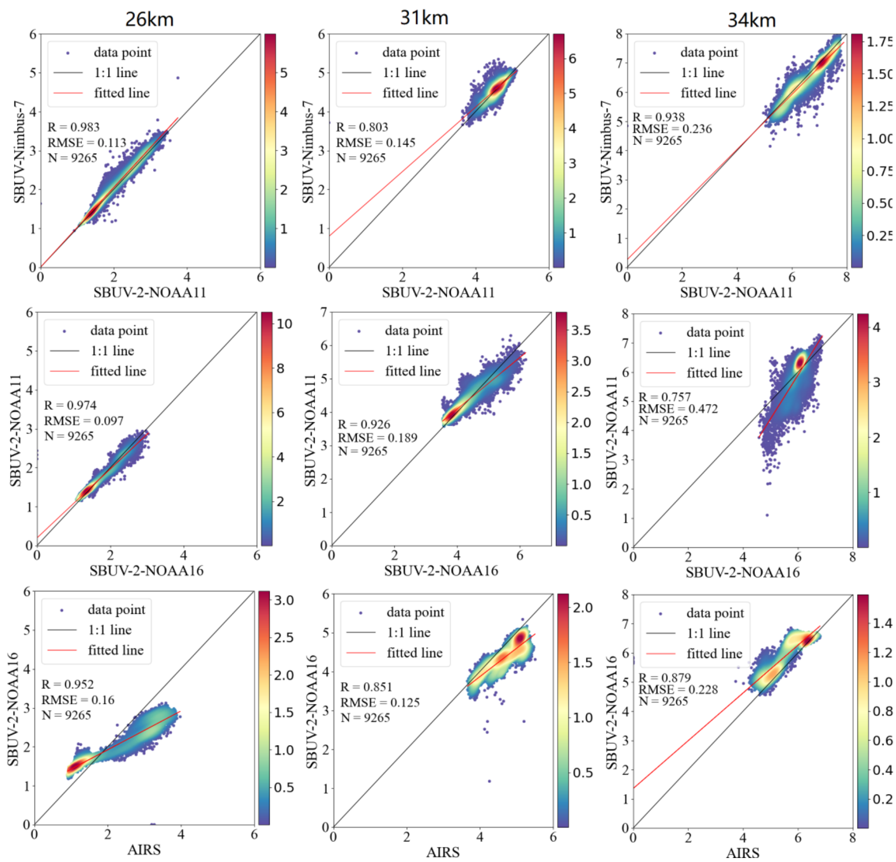

Fig. 6. Similar to Figure 4 but for the satellite datasets after CDF match. The first to third rows indicate the comparison results of calibrated Nimbus-7-SBUV vs. calibrated NOAA11-SBUV-2, calibrated NOAA11-SBUV-2 vs. calibrated NOAA16-SBUV-2, and calibrated NOAA16-SBUV-2 vs. AIRS, respectively.

From the above results, it can be seen that the effectiveness of CDF matching depends on the situation. It generally significantly improves the agreement between two satellite datasets when there are large deviations between them. However, if the agreement between two datasets is already good, the improvement of CDF matching is very slight. Particularly, CDF matching does not always work well in some cases and should be used with caution. Regarding the satellite datasets used in this study, CDF matching generally play a positive role in improving the consistency between different satellite datasets. Thus, the four datasets after CDF matching were used to construct the

https://doi.org/10.5194/amt-2022-282
Preprint. Discussion started: 14 October 2022

long-term and consistent ozone datasets.

4.3 Ozone distribution

4.3.1 The vertical distribution of ozone

The ozone profile of China was established using the linear interpolation of 28 spatial mean values at the height from 0 km to 80 km with intervals of 1 km. The unit of ozone digital density which is transferred from the ozone mixing ratio using temperature datasets of AIRS, was adopted because it is more sensitive to subtle changes. Fig. 7 shows the superimposed display of ozone profile in China from 2003 to 2020. Compared to the ozone profile in troposphere extracted by TROPOMI (Zhao et al., 2020), the ozone profile extracted by AIRS present larger variation trend throughout the troposphere, indicating that AIRS can capture more details in the troposphere. This occurs because TROOMI has more sparse records in the troposphere. Additionally, the inconsistent unit of ozone between them (i.e., the former used ppmv) while the latter used ozone digital density) may also contribute to the difference between them.

The ozone digital density varies significantly with height. Its value is close to 0 at the top of the stratosphere. Then it increases significantly and reaches the maximum of about $2.5*10^{12}/cm^3$ at 34 km. From then on, the ozone digital density decreases significantly with the reduction of height and reaches a minimum of about $3*10^{11}/cm^3$ at the bottom of stratosphere. The variation trend of ozone with height in the troposphere is similar to that of the stratosphere. The ozone digital density is relatively low in the upper stratosphere. Then it increases gradually with the reduction of the height and reaches the maximum of $6*10^{11}/cm^3$ at the height of 3 km, from which it decreases gradually with the degression of height.

Fig. 7 further shows that the interannual variation trend of ozone above 50 km is nearly zero since the ozone profiles of different years completely overlapped. But it tends to increase with the reduction of height and arrives the maximum at the height around 34 km, since the differences between these ozone profiles increase gradually as height decreases. Particularly, the ozone digital density at the height around 34 km shows a significant downward trend by $3*10^{11}$/cm3 from 2003 to 2020. The interannual variation of ozone reduce slightly from 31 km to 26 km. But as the height decrease from 26 km to 24 km, the downward trend becomes larger. With the further decrease of height until 10 km, the interannual variation of ozone is basically stable. But after that, interannual variation of ozone tends to increase and reaches the maximum at the 5 km. The interannual variation of ozone below 3 km is very small. In this study, we selected

https://doi.org/10.5194/amt-2022-282
Preprint. Discussion started: 14 October 2022

Atmospheric Measurement Techniques
Open Access
EGU
Discussions

ozone at 6 height levels (i.e., 3 km, 5 km, 6 km, 31 km, and 34 km) to explore the spatiotemporal variation of ozone in China, because relatively large interannual variabilities were observed at these heights. The height of 12 km was also selected because it is the top of the troposphere.

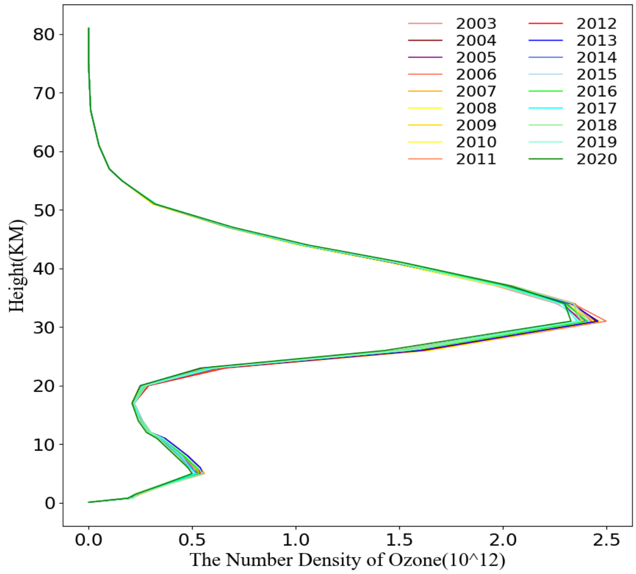

Fig. 7. The ozone profile of China from 2003 to 2020 extracted from AIRS.

4.3.2 Ozone distribution and variation (1978-2020)

4.3.2.1 The monthly variation of ozone at different altitudes

In order to show the monthly variation of ozone at the six altitudes, Fig. 8 presents the boxplots of the monthly ozone from 1978. The ozone in the troposphere presents obvious seasonal variations (Fig. 8(a-c)). Furthermore, the seasonal variations of ozone at the height of 3 km and 5 km are very similar, with the "positive-negative-positive-negative" tendency from January to December. The ozone presents the smallest values (around 0.052 ppmv and 0.58 ppmv at the height of 3 km and 5 km, respectively) in January, March, and April, and the largest values (about 0.072 ppmv and 0.085 ppmv at the height of 3 km and 5 km, respectively) in August and September. By contrast, the ozone at the height of 12 km shows a different seasonal variation characteristic. An abnormal high value occurs in January, with values around 0.112 ppmv. Then a "positive-negative" tendency can be seen, with the peak of about 0.115 ppmv appearing in May and June. The minimum value of about 0.083 ppmv appears in February and December. Regarding the interannual variations of ozone, there is a big change of the

https://doi.org/10.5194/amt-2022-282
Preprint. Discussion started: 14 October 2022

interannual variation of ozone between different months. At the heights of 3 km and 5 km, the interannual variation of trend is relatively small in January, March, and April, but large in May and June. By contrast, the ozone at the height of 12 km shows large interannual variations in January, April, May, June, and July, but small interannual variations in other months. The seasonal trend of ozone in China presented here is consistent with that indicated by IAGOS in the Tropospheric Ozone Assessment Report (TOAR) (Galdel et al., 2018), which reported that the ozone content in the middle and upper troposphere in China began to rise from March to May, reached the peak from June to September, and returned to a low level from October to December. In the lower troposphere (2-3 km), the ozone content reached the peak in summer.

Unlike the troposphere, the seasonal variation of ozone is not obvious in the stratosphere (Fig. 8(d-f)). It is noteworthy that the ozone in January remains to be high in the height of 26 km and 31 km, with values of about 2.6 ppmv and 4.6 ppmv, respectively. At the height of 26 km, the ozone from February to June is generally larger than that from July to December. The former ranges from 2.3 ppmv to 2.4 ppmv, while the latter ranges from 2.0 ppmv to 2.2 ppmv. By contrast, there is no obvious difference of the ozone at the height of 31 km from February to December, with the values ranging from 4.35 ppmv to 4.5 ppmv. When the height of 34 km was considered, the ozone in January shows the minimum values of about 5.65 ppmv throughout the year. A “negative-positive-negative” tendency can be observed, and the inflection point appear in April and September. Compared to the ozone in the troposphere, the ozone in the stratosphere consistently shows larger interannual variability throughout different months, as indicated by the wide spread of the boxplots (Fig. 8(d-f)). Particularly, the interannual variations are larger in February, March, May, June, July, and December than other months at the height of 26 km. But when it comes to the height of 31 km, the interannual variations are relatively larger from December to May than other months. At the height of 34 km, the interannual variations are more significant in January, April, May, June, and July.

https://doi.org/10.5194/amt-2022-282
Preprint. Discussion started: 14 October 2022

Atmospheric Measurement Techniques
Discussions

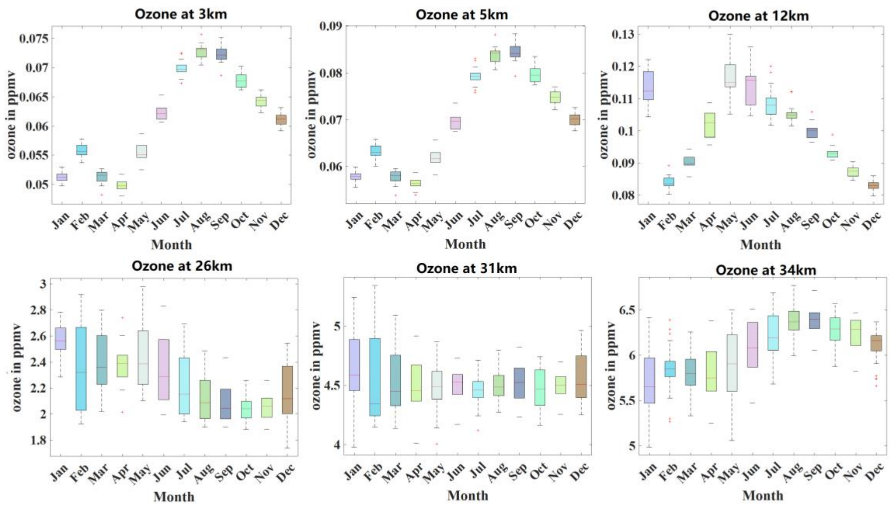

Fig. 8. Monthly variations of ozone in China from 1978 to 2020. (a)-(f) denote the variation at the heights of 3 km, 5 km, 12 km, 26 km, 31 km, and 34 km, respectively.

From the above results, it can be concluded that the seasonal variation of ozone is more significant in the troposphere than that in the stratosphere. But the interannual variation of ozone is larger in the stratosphere than that in the troposphere. Despite the obvious seasonal variation of ozone in the troposphere, the month when peak appears show dependence on height. Particularly, the seasonal and interannual variation characteristics of zone at the height of 3 km and 5 km are almost the same. It is noteworthy that in the top of the tropopause (i.e., the height of 12 km), the ozone is unusually high in January. This may be caused by the vertical downward transmission of zone in the stratospheric under the context of weakened atmospheric circulation (McCormack and Hood, 1996; Liu et al., 2020).

https://doi.org/10.5194/amt-2022-282
Preprint. Discussion started: 14 October 2022

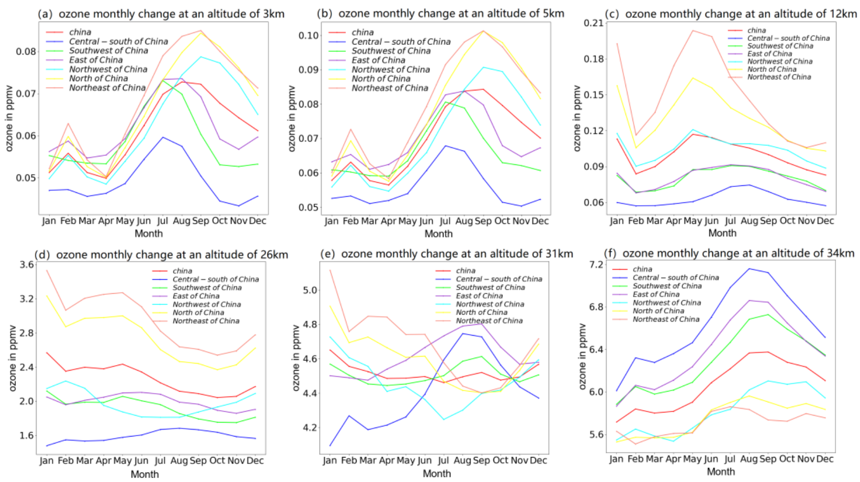

Fig. 9. Monthly variations of ozone over the six administrative zoning areas of China from 1978 to 2020. (a)-(f) denote the results at the heights of 3 km, 5 km, 12 km, 26 km, 31 km, and 34 km, respectively.

In order to show the ozone distribution characteristics over different regions of China, the multi-year averaged monthly ozone is displayed for different regions in Fig. 9. Additionally, the multi-year averaged monthly ozone over the whole China is also presented. These six regions all show consistent seasonal variations of ozone, but the time when peak and valley appear show dependence on different regions. At the height of 3 km and 5 km (Fig. 9(a-b)), the central-south, southwest, and east China present the maximum ozone in July, which is earlier than that of northeast, north, and northwest China, which present the maximum ozone in September. Nevertheless, an opposite phenomenon can be found at the height of 12 km (Fig. 9(c)), where the former group present the maximum ozone in August, which is later than the latter group, which present the maximum ozone in May. Regarding the magnitude of ozone in the troposphere, northeast and north China generally present higher ozone than the national average, while the central south of China presents the lowest ozone among these regions throughout the year.

When it comes to the stratosphere, the ozone content in different regions has obvious stratification at the height of 26 km and 34 km. It is interesting to find that the rank of these regions regarding the magnitude of ozone content are almost opposite between the heights of 26 km and 34 km. At the height of 26 km, the northeast China presents the largest ozone content throughout the year, followed by north China, and central south China ranks the last among these six regions (Fig. 9(d)). By contrast, at the height of 34 km, central south China shows the largest ozone content throughout the year, and northeast and north China present the smallest ozone content. This result

https://doi.org/10.5194/amt-2022-282
Preprint. Discussion started: 14 October 2022

demonstrates that the effects of atmospheric circulation are significantly different at different altitudes of stratosphere. Although the national averaged ozone does not show obvious month-to-month variations at the height of 31 km, the subregion presents significant seasonal variability (Fig. 9(e)). Particularly, the variation characteristics of ozone over the six regions tend to polarize into two groups at this height: (1) the northeast, north, and northwest China; (2) the central-south, southwest, and east China. The two groups basically present an opposite seasonal variation trend. The order of these regions regarding the magnitude of ozone content is not fixed given that the lines in Fig. 9(e) interweave with each other.

When the results of the stratosphere and troposphere are combined, it can be found that below the height of 26 km, northeast and north China show higher ozone content than the national average. By contrast, central-south, southwest, and east China present lower ozone content than the national average. But an opposite phenomenon appears at the height of 34 km. This occurs because the latitude of east and central-south China is relatively low, which weakened the impact of atmospheric circulation but enhanced the impact of solar radiation. This phenomenon indicates that atmospheric circulation is a main influencing factor of ozone distribution at lower altitudes. By contrast, temperature and solar radiation are dominant factors of zonal distribution at higher altitudes (McCormack and Hood, 1996).

4.3.2.2 The detection and mapping of the changing trend of ozone

In order to show the spatiotemporal variation of ozone at different altitudes, we present the multi-year (1978-2020) annual-averaged ozone, the standard deviation of the annual ozone throughout these years, and the interannual variation trend of ozone at the three altitudes in the stratosphere in Fig. 10. It can be seen that the distribution characteristics of the multi-year annual averaged zone at the height of 34 km is totally different or even opposite to those at the heights of 31 km and 26 km, which is consistent with the results in Fig. 9. At the height of 34 km, it can be seen that the ozone content in low latitudes (i.e., southeast and southwest China) is significantly higher than that in high latitudes (i.e., northeast and northwest China), with the maximum difference of 2.8 ppmv. This finding disagrees with Li et al. (2019), which demonstrated that the total ozone content increases with the increase of latitude. The discrepancy can be explained by the fact that the results we present is only for the height of 34 km while the previous study is focused on the whole atmosphere. Regarding the standard deviation of ozone (Fig. 10(b)), the east and northwest China show larger values than other areas, indicating that larger temporal fluctuations exist over these areas. From Fig. 10(c), it can be seen that 87.1 % of China presents an upward trend from 1978 to 2020, which is mainly distributed over northwestern China, with the maximum value

https://doi.org/10.5194/amt-2022-282
Preprint. Discussion started: 14 October 2022

Atmospheric Measurement Techniques
Open Access
Discussions

of 0.009 ppmv yr^{-1}. 12.9% of China shows a downward trend, which is mainly distributed over eastern China, with the maximum of -0.0045 ppmv yr^{-1}.

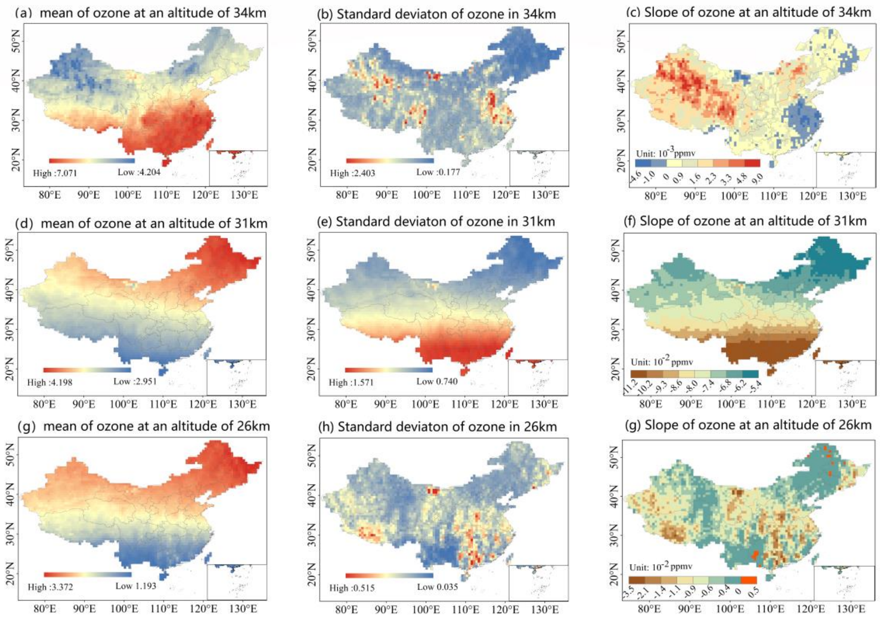

Fig. 10. Spatial distribution map of the multi-year (1978-2020) annual-averaged ozone (left), the standard deviation of annual ozone (middle), and the interannual variation trend (left) in the stratosphere. The first to the third lines refer to the results at the height of 34 km, 31 km, and 26 km, respectively.

The multi-year annual-averaged ozone at the heights of 31 km and 26 km present a similar spatial distribution characteristic, which increases gradually with latitude and comply with the general variation laws. However, it is noteworthy that the distribution characteristic of the standard deviation is even opposite to the multi-year annual average at the height of 31 km (Fig. 10(e) vs. Fig. 10(d)). The areas with large ozone content present a small standard deviation, and the standard deviation of the area with low-ozone is large. This demonstrates that the temporal fluctuations in high-ozone areas are small, and vice versa. The ozone at the height of 31 km presents a decreasing trend from 1978 to 2020 throughout China (Fig. 10(f)). Furthermore, the magnitude of the interannual trends decreases with latitude, which is similar to that of the standard deviation. Despite the similar distribution characteristics of the multi-year annual-averaged ozone at the heights of 31 km and 26 km, there is a big difference regarding the distributions of the standard deviation and interannual trends (Fig. 10(h-g)). The standard deviation at the height of 26 km present larger spatial heterogeneity, with larger values over central-south and east China. Particularly, the regions of Inner

https://doi.org/10.5194/amt-2022-282
Preprint. Discussion started: 14 October 2022

Atmospheric Measurement Techniques
Discussions

Mongolia present significantly larger standard deviation than their surroundings (Fig. 10(h)), which is similar to that of 31 km and 34 km (Fig. 10(b and e)). The ozone content at the height of 26 km mainly shows a downward interannual trend, which occupies 99.3% of China. And only 0.7% of China presents positive trend ranging from 0.003 and 0.009 ppmv yr^{-1}.

From the above analysis, it can be concluded that both the spatial distribution characteristics of the multi-year annual averaged ozone and the interannual trend show strong dependence on the altitude in the stratosphere. Different altitude may lead to completely opposite results. This agrees well with the work by Ball et al. (2018), which demonstrated that the ozone in the middle stratosphere continues to recover while the ozone in the lower stratosphere continues to decrease. Therefore, caution should be exercised in the interpretation of the spatiotemporal variation of ozone in the stratosphere. It is noteworthy that although some areas of China show an increase trend at the height of 34 km with the maximum of 0.009 ppmv yr^{-1}, the decreasing trend at the height of 31 km can reach 0.055 ppmv yr^{-1}, which is much larger than the increase rate of ozone at 34 km. This demonstrates that when studying whether the total ozone content in the stratosphere has recovered in the past years, the increase of ozone content in the upper stratosphere may be offset by the decrease of ozone content in the lower stratosphere. Regarding the trend detection of ozone in the stratosphere, a more detailed division of stratospheric ozone is needed, and the internal driving factors of such characteristics need to be further explored.

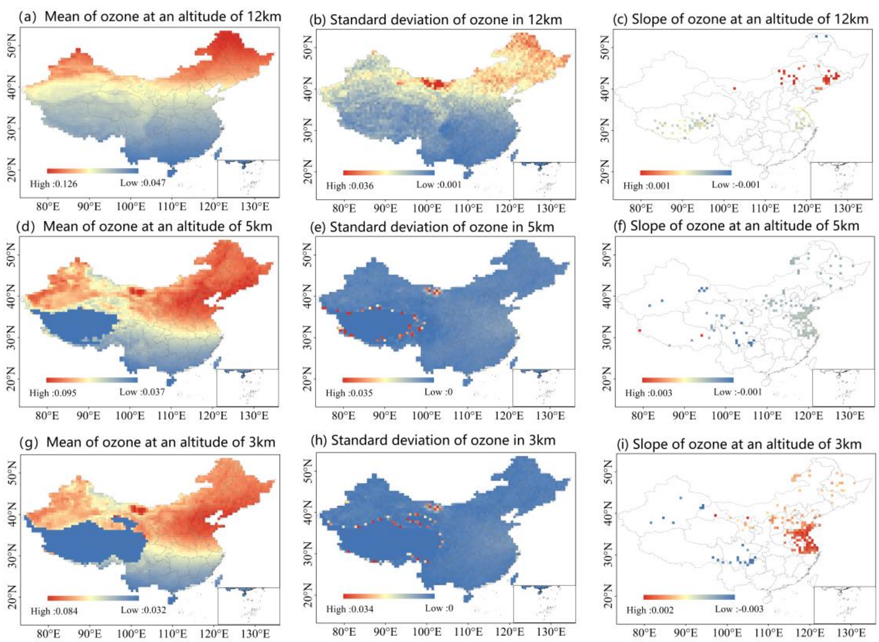

https://doi.org/10.5194/amt-2022-282
Preprint. Discussion started: 14 October 2022

Fig. 11. Spatial distribution map of the multi-year (2003-2020) annual averaged ozone (left), the standard deviation of ozone in the time dimension (middle), and the interannual variation trend (left) in the troposphere. The first to the third lines refer to the results at the height of 12 km, 5 km, and 3 km, respectively.

When the ozone at the top of the troposphere is focused (Fig. 11(a-b)), it can be seen that the multi-year annual averaged ozone and the standard deviation show similar but distinct latitude-belt distribution characteristics, with low values at the low latitude and large values at high latitude. This demonstrates that the areas with large ozone tend to present larger temporal fluctuations in the top of the troposphere, and vice versa.

The height of 5 km and 3 km show similar spatial distribution characteristics in terms of the multi-year annual averaged ozone and the standard deviation of ozone content (Fig. 11(d-i)). Nevertheless, two special areas, i.e., Qinghai Tibet Plateau (QTP) and north China plain, show large differences from their surroundings regarding the magnitude of the multi-year annual averaged ozone. The QTP shows the lowest ozone throughout China, with the value of 0.037 ppmv and 0.032 ppmv at the height of 5 km and 3 km, respectively. Furthermore, the ozone spatial distribution in QTP is rather homogeneous. By contrast, significantly high ozone appears in the north China plain, with a maximum of 0.095 ppmv and 0.084 ppmv (~ 180.1 ug/m^3) at the height of 5 km and 3 km, respectively. But this does occur in the height of 12 km. Another noticeable feature is that the ozone content in the eastern part of Ejina Banner Inner Mongolia is much greater than their surroundings at the three heights.

In terms of the standard deviations at the heights of 5 km and 3 km, it can be seen that they are almost evenly distributed across the country except for QTP and north China plain. Moreover, it is interesting to find that there are a series of high values which sporadically distributed at the marginal areas of QTP. This happens because the ozone in India and Southeast Asia is blocked by QTP when it was transmitted in space, resulting in high values and high standard deviations in the marginal area (Li, 2020). Regarding the interannual trend of ozone in the troposphere, most areas in China do not pass the Mann-Kendall test with the confidence level of 95% at these heights. Only north China and East China show an upward trend at the heights of 3 km and 5 km. The upward trend over north China is contrast with Dufour et al. (2018), who found a significant downward trend from 2012 to 2016 based on IASI dataset from 2008 to 2016. This inconsistency may be the result of longer time series of dataset (2003-2020) we used. Our results demonstrate that the ozone in North China Plain shows an increasing trend of about 0.1 ppb yr^{-1}.

From the above analysis, it can be seen that the interannual variation of ozone in the troposphere is not as significant as that of stratosphere. In particular, the standard deviation of ozone between different years are very small at the height of 5 km and 3

https://doi.org/10.5194/amt-2022-282
Preprint. Discussion started: 14 October 2022

Atmospheric Measurement Techniques
Discussions

km, indicating that the ozone content near the ground is relatively stable in the past years. The significant regional characteristics of QTP at the height of 5 km and 3 km do not appear at other altitude levels. The large ozone content in the northeast China is noticeable, because it will cause a significant increase in near-ground ozone when ozone is transported downward by convection.

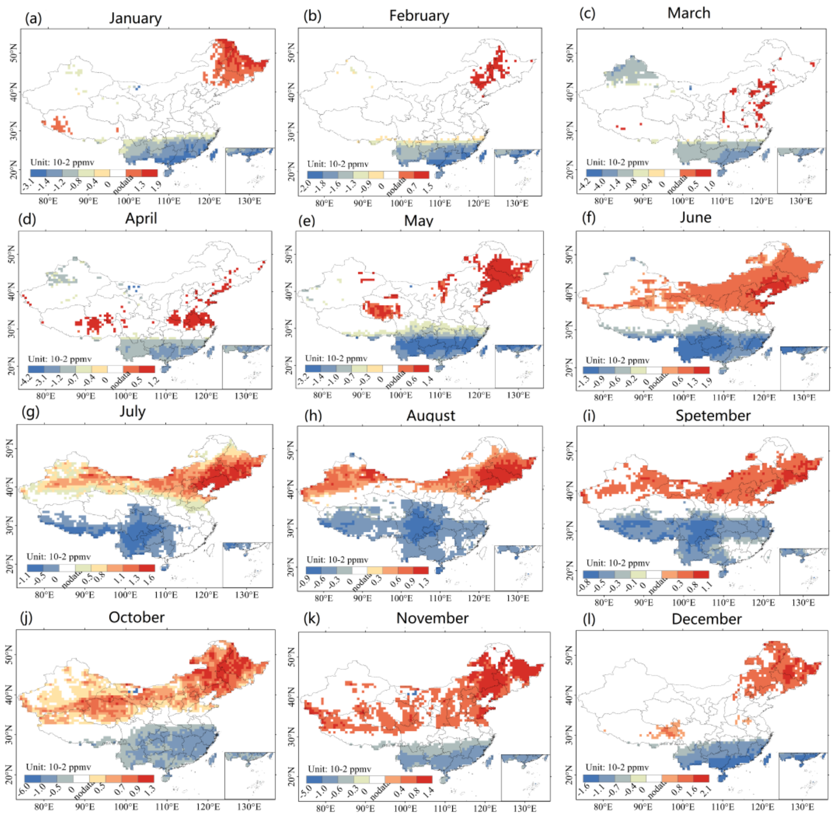

Fig. 12. Spatial distribution of the interannual trend of ozone from 1978 to 2020 for different months at the height of 26 km.

Given the significant interannual variation trend in the stratosphere, we present the interannual trends from January to December in order to investigate which month dominates the interannual variations of ozone (Fig. 12). Here, the height of 26 km was selected since it is the lower stratosphere and affected by both solar radiation and atmospheric circulation. It can be seen that the interannual trend of ozone show strong dependence on months, with large difference of the magnitude of trend between different months. But the spatial distribution of the interannual trends on the monthly scale is basically consistent between different months, which present obvious latitude-belt distribution characteristics, with positive trend in the north of 40 N° and negative

https://doi.org/10.5194/amt-2022-282
Preprint. Discussion started: 14 October 2022

trend in the south of 28 N°. This result disagrees with that on the yearly scale (Fig. 10(g)). This occurs because the interannual trend of ozone on the yearly scale is a combination of the variation of different months. From Fig. 12, it can be found that more than 60% of China show significant interannual trend from June to October, but only small areas passed the 95% confidence test in other months.

5. Conclusion

This study performs a long-term detection, mapping, and interpretation of ozone in the stratosphere and troposphere. The quality of different satellite ozone datasets has been taken into account through the direct comparison with *in-situ* data and the cross-calibration between different satellite datasets. Finally, a long-term consistent ozone dataset from 1978 to 2020 was constructed. Based on the ozone profile of China, six heights with obvious interannual variations were selected from the troposphere and stratosphere to present the results. Several conclusions can be drawn from the present results:

(1) AIRS ozone dataset basically agrees with *in-situ* observations and has the ability to reveal the spatiotemporal distribution characteristics of ozone. The consistency between NOAA11-SBUV-2 and NOAA16-SBUV-2 is the best, followed by Nimbus-7-SBUV and NOAA11-SBUV-2. And that of NOAA16-SBUV-2 vs. AIRS ranks last. The best agreement of the satellite datasets occurs at the height of 26 km.

(2) The effectiveness of CDF matching is more significant when there are large deviations between the two datasets, but slight if the agreement between two datasets is already good. Overall, it plays a positive role in improving the consistency between different satellite datasets.

(3) The seasonal variation of ozone is more significant in the troposphere than that of the stratosphere. But the interannual variation of ozone is larger in the stratosphere than that of the troposphere. The unusually high ozone at the top of the troposphere in January is noteworthy. This may be the result of the vertical downward transmission of stratospheric ozone under the context of weakened atmospheric circulation.

(4) Below the height of 26 km, the northeast and north China show higher ozone content than the national average, while the central-south, southwest, and east China present lower ozone content than the national average. But an opposite phenomenon appears at the height of 34 km.

(5) The spatiotemporal distribution of ozone in the stratosphere shows a strong dependence on altitudes. Different altitudes may lead to completely opposite results. The increase of ozone content in the upper stratosphere may be offset by the

decrease of ozone content in the lower stratosphere. Thus, the altitude should be a major consideration when studying whether the total ozone content in the stratosphere has recovered in the past years.

(6) The interannual variation of ozone in the troposphere is not as significant as that of the stratosphere. The ozone content near the ground is relatively stable in the past years. But the large ozone content in northeast China is noticeable since it will cause a significant increase in near-ground ozone when ozone is transported downward by convection. Particularly, the distinct regional distribution characteristics (i.e., lowest ozone throughout China and spatially homogeneous distribution) over QTP is noticeable, which only appear in the near ground (i.e., 5 km and 3 km).

Data Availability

The ozone profile datasets of satellites over the study area are freely available at https://daac.gsfc.nasa.gov/datasets/AIRS2RET_7.0/summary?keywords=AIRS and https://daac.gsfc.nasa.gov/datasets?keywords=SBUV&page=1. The in-situ ozone dataset can be accessed at https://quotsoft.net/air/#messy by searching the date.

Author contributions

Rongqi Tang and Xiaodan Wu planned the research; Rongqi Tang and Xiaodan Wu analyzed the data; Rongqi Tang, Xiaodan Wu wrote the manuscript draft; Jingping Wang, Dujuan Ma, Qicheng Zeng, Jianguang Wen, and Qing Xiao reviewed and edited the manuscript.

Competing interests

The authors declare that they have no conflict of interest.

Acknowledgments

This work was supported in part by the National Natural Science Foundation of China under Grant 42071296, and in part by the China High-Resolution Earth Observation System under Grant 21-Y20B01-9001-19/22.

Reference:

Andersen, S. O., & Sarma, K. M. (2012). Protecting the ozone layer: the United Nations history. Routledge. DOI: 10.4324/9781849772266

Bian, J., Gettelman, A., Chen, H., & Pan, L. L. (2007). Validation of satellite ozone profile retrievals using Beijing ozonesonde data. Journal of Geophysical Research: Atmospheres, 112(D6). DOI: 10.1029/2006JD007502

Blackwell, W. J. (2012). Neural network Jacobian analysis for high-resolution profiling of the atmosphere. EURASIP Journal on Advances in Signal Processing, 2012(1), 1-11.

Blackwell, W. J., & Milstein, A. B. (2014). A neural network retrieval technique for high-resolution profiling of cloudy atmospheres. IEEE Journal of Selected Topics in Applied Earth Observations and Remote Sensing, 7(4), 1260-1270. DOI: 10.1109/JSTARS.2014.2304701

Ball, W. T., Alsing, J., Mortlock, D. J., Staehelin, J., Haigh, J. D., Peter, T., ... & Rozanov, E. V. (2018). Evidence for a continuous decline in lower stratospheric ozone offsetting ozone layer recovery. Atmospheric Chemistry and Physics, 18(2), 1379-1394. DOI: 10.5194/acp-18-1379-2018

Chen, L., Yu, B., Chen, Z., Li, B., & Wu, J. (2014). Investigating the temporal and spatial variability of total ozone column in the Yangtze River Delta using satellite data: 1978–2013. Remote Sensing, 6(12), 12527-12543. DOI: 10.3390/rs61212527

Cazorla, M., Parra, R., Herrera, E., & da Silva, F. R. (2021). Characterizing ozone throughout the atmospheric column over the tropical Andes from in situ and remote sensing observations. Elem Sci Anth, 9(1), 00019. DOI: 10.1525/elementa.2021.00019

Dufour, G., Eremenko, M., Beekmann, M., Cuesta, J., Foret, G., Fortems-Cheiney, A., ... & Zhang, Y. (2018). Lower tropospheric ozone over the North China Plain: variability and trends revealed by IASI satellite observations for 2008–2016. Atmospheric Chemistry and Physics, 18(22), 16439-16459. DOI: 10.5194/acp-18-16439-2018

Evan Manning, J. P. L., Larrabee Strow, U. M. B. C., Teixeira, J., Leader, J. A. T., Fetzer, E. J., Yue, Q., & Thrastarson, H. T. (2020). AIRS-Team Retrieval For Core Products and Geophysical Parameters: Versions 6 and 7 Level 2. Jet Propulsion.

Fishman, J., Ramanathan, V., Crutzen, P. J., & Liu, S. C. (1979). Tropospheric ozone and climate. Nature, 282(5741), 818-820.

Frith, S. M., Kramarova, N. A., Stolarski, R. S., McPeters, R. D., Bhartia, P. K., & Labow, G. J. (2014). Recent changes in total column ozone based on the SBUV Version 8.6 Merged Ozone Data Set. Journal of Geophysical Research: Atmospheres, 119(16), 9735-9751.

Gaudel, A., Cooper, O. R., Ancellet, G., Barret, B., Boynard, A., Burrows, J. P., ... & Lewis, A. (2018). Tropospheric Ozone Assessment Report: Present-day distribution and trends of tropospheric ozone relevant to climate and global atmospheric chemistry model evaluation. Elementa: Science of the Anthropocene, 6. DOI: 10.1525/elementa.291

Huang, J. P., Fung, J. C., & Lau, A. K. (2006). Integrated processes analysis and systematic meteorological classification of ozone episodes in Hong Kong. Journal of Geophysical Research: Atmospheres, 111(D20). DOI: 10.1029/2005JD007012

Huang, C., Chen, C. H., Li, L., Cheng, Z., Wang, H. L., Huang, H. Y., ... & Chen, Y. R.

Atmospheric Measurement Techniques Discussions
Open Access EGU

(2011). Emission inventory of anthropogenic air pollutants and VOC species in the Yangtze River Delta region, China. Atmospheric Chemistry and Physics, 11(9), 4105-4120. DOI: 10.5194/acp-11-4105-2011

Hulswar, S., Mohite, P., Soni, V. K., & Mahajan, A. S. (2021). Differences between in-situ ozonesonde observations and satellite retrieved ozone vertical profiles across Antarctica. Polar Science, 100688. DOI: 10.1016/j.polar.2021.100688

Jerrett, M., Burnett, R. T., Pope III, C. A., Ito, K., Thurston, G., Krewski, D., ... & Thun, M. (2009). Long-term ozone exposure and mortality. New England Journal of Medicine, 360(11), 1085-1095. DOI: 10.1056/NEJMoa0803894

Kondratyev, K. Y., & Varotsos, C. A. (1996). Global total ozone dynamics. Environmental Science and Pollution Research, 3(3), 153-157.

Kondratyev, K. Y., & Varotsos, C. (2002). Remote sensing and global tropospheric ozone observed dynamics. International Journal of Remote Sensing, 23(1), 159-178. DOI: 10.1080/01431160010014765

Kilifarska, N. A. (2012). Mechanism of lower stratospheric ozone influence on climate. International Review of physics, 6(3), 279-290.

Liu, Y. Y., Parinussa, R. M., Dorigo, W. A., De Jeu, R. A., Wagner, W., Van Dijk, A. I. J. M., ... & Evans, J. P. (2011). Developing an improved soil moisture dataset by blending passive and active microwave satellite-based retrievals. Hydrology and Earth System Sciences, 15(2), 425-436. DOI: 10.5194/hess-15-425-2011

Li, X., Li, Y. J., Ma, Q. M., Chen, J., Chen, F., Yang, X. Y., & Wang, Q. J. (2019). Spatial and Temporal Variation of Total and Tropospheric Ozone Columns Over China. The International Archives of Photogrammetry, Remote Sensing and Spatial Information Sciences, 42, 113-118.

Li, J. (2020). Pollution trends in China from 2000 to 2017: A multi-sensor view from space. Remote Sensing, 12(2), 208. DOI: 10.3390/rs12020208

Liu, J., Rodriguez, J. M., Oman, L. D., Douglass, A. R., Olsen, M. A., & Hu, L. (2020). Stratospheric impact on the Northern Hemisphere winter and spring ozone interannual variability in the troposphere. Atmospheric Chemistry and Physics, 20(11), 6417-6433. DOI: 10.5194/acp-20-6417-2020

Maddy, E. S., & Barnet, C. D. (2008). Vertical resolution estimates in version 5 of AIRS operational retrievals. IEEE Transactions on Geoscience and Remote Sensing, 46(8), 2375-2384.

Ma, P., Mao, H., Zhang, J., Yang, X., Zhao, S., Wang, Z., ... & Chen, C. (2022). Satellite monitoring of stratospheric ozone intrusion exceptional events-a typical case of China in 2019. Atmospheric Pollution Research, 13(2), 101297. DOI: 0.1016/j.apr.2021.101297

MEPC (Ministry of Environmental Protection of China), 2013 MEPC (Ministry of

https://doi.org/10.5194/amt-2022-282
Preprint. Discussion started: 14 October 2022

Atmospheric Measurement Techniques Discussions

Environmental Protection of China) Technical regulation for selection of ambient air quality monitoring stations (on trial), http://www.cnemc.cn/publish/totalWebSite/news/news_38841.html , 2013.

McCormack, J. P., & Hood, L. L. (1996). Apparent solar cycle variations of upper stratospheric ozone and temperature: Latitude and seasonal dependences. Journal of Geophysical Research: Atmospheres, 101(D15), 20933-20944. DOI: 10.1029/96JD01817

Meijer, Y. J., & Kelder, H. M. (2006). Publications, presentations and other activities Evaluation of Global Ozone Monitoring Experiment (GOME) ozone profiles from nine different algorithms 2006. J. Geophys. Res, 111. DOI: 10.1029/2005JD006778

Meier, W. N., Stroeve, J., & Fetterer, F. (2007). Whither Arctic sea ice? A clear signal of decline regionally, seasonally and extending beyond the satellite record. Annals of Glaciology, 46, 428-434. DOI: 10.3189/172756407782871170

McPeters, R. D., Bhartia, P. K., Haffner, D., Labow, G. J., & Flynn, L. (2013). The version 8.6 SBUV ozone data record: An overview. Journal of Geophysical Research: Atmospheres, 118(14), 8032-8039.

Ohyama, H., Kawakami, S., Shiomi, K., & Miyagawa, K. (2011). Retrievals of total and tropospheric ozone from GOSAT thermal infrared spectral radiances. IEEE transactions on geoscience and remote sensing, 50(5), 1770-1784. DOI: 10.1109/TGRS.2011.2170178

Rawat, P., Naja, M., Fishbein, E., Thapliyal, P. K., Kumar, R., Bhardwaj, P., ... & Lal, S. (2022). Performance of AIRS ozone retrieval over the central Himalayas: Case studies of biomass burning, downward ozone transport and radiative forcing using long-term observations. Atmospheric Measurement Techniques Discussions, 1-59.

Ramanathan, V., & Dickinson, R. E. (1979). The role of stratospheric ozone in the zonal and seasonal radiative energy balance of the earth-troposphere system. Journal of Atmospheric Sciences, 36(6), 1084-1104. DOI:10.1175/1520-0469(1979)036<1084:TROSOI>2.0.CO;2

Ramanathan, V., & Feng, Y. (2009). Air pollution, greenhouse gases, and climate change: Global and regional perspectives. Atmospheric Environment, 43(1), 37-50. DOI: 10.1016/j.atmosenv.2008.09.063

Sellitto, P., Bojkov, B. R., Liu, X., Chance, K., & Frate, F. D. (2011). Tropospheric ozone column retrieval at northern mid-latitudes from the Ozone Monitoring Instrument using a neural network algorithm. Atmospheric Measurement Techniques, 4(11), 2375-2388. DOI: 10.5194/amt-4-2375-2011

Silver, B., Reddington, C. L., Arnold, S. R., & Spracklen, D. V. (2018). Substantial changes in air pollution across China during 2015–2017. Environmental Research

Letters, 13(11), 114012. DOI: 10.1088/1748-9326/aae718

Treshow, M. (1970). Ozone damage to plants. Environmental Pollution (1970), 1(2), 1 55-161. DOI: 10.1016/0013-9327(70)90016-9

Tao, Z., Blackwell, W. J., & Staelin, D. H. (2012). Error variance estimation for individual geophysical parameter retrievals. IEEE transactions on geoscience and remote sensing, 51(3), 1718-1727. DOI: 10.1109/TGRS.2012.2207728

Wang, T., Xue, L., Brimblecombe, P., Lam, Y. F., Li, L., & Zhang, L. (2017a). Ozone pollution in China: A review of concentrations, meteorological influences, chemical precursors, and effects. Science of the Total Environment, 575, 1582-1596. DOI: 10.1016/j.scitotenv.2016.10.081

Wang, W. N., Cheng, T. H., Gu, X. F., Chen, H., Guo, H., Wang, Y., ... & Zhang, X. C. (2017b). Assessing spatial and temporal patterns of observed ground-level ozone in China. Scientific reports, 7(1), 1-12. DOI: 10.1038/s41598-017-03929-w

Wargan, K., Orbe, C., Pawson, S., Ziemke, J. R., Oman, L. D., Olsen, M. A., ... & Emma Knowland, K. (2018). The recent decline in extratropical lower stratospheric ozone is attributed to circulation changes. Geophysical research letters, 45(10), 5166-5176. DOI: 10.1029/2018GL077406

Wang, H., Chai, S., Tang, X., Zhou, B., Bian, J., Vömel, H., ... & Wang, W. (2019). Verification of satellite ozone/temperature profile products and ozone effective height/temperature over Kunming, China. Science of The Total Environment, 661, 35-47. DOI: 10.1016/j.scitotenv.2019.01.145

Wang, S., Zhang, Y., Ju, W., Chen, J. M., Cescatti, A., Sardans, J., ... & Peñuelas, J. (2021). Response to Comments on "Recent global decline of CO2 fertilization effects on vegetation photosynthesis". Science, 373(6562), eabg7484. DOI: 10.1126/science.abg7484

Yue, X., & Unger, N. (2014). Ozone vegetation damage effects on gross primary prod uctivity in the United States. Atmospheric Chemistry and Physics, 14(17), 9137-9153. DOI: 10.5194/acp-14-9137-2014

Yin, C. Q., Solmon, F., Deng, X. J., Zou, Y., Deng, T., Wang, N., ... & Liu, L. (2019). Geographical distribution of ozone seasonality over China. Science of the Total Environment, 689, 625-633. DOI: 10.1016/j.scitotenv.2019.06.460

Zhang, Q., Cheng, J., & Liang, S. (2018). Deriving high-quality surface emissivity spectra from atmospheric infrared sounder data using cumulative distribution function matching and principal component analysis regression. Remote Sensing of Environment, 211, 388-399. DOI: 10.1016/j.rse.2018.04.033

Zhao, F., Liu, C., Cai, Z., Liu, X., Bak, J., Kim, J., ... & Liu, J. (2021). Ozone profile retrievals from TROPOMI: Implication for the variation of tropospheric ozone

https://doi.org/10.5194/amt-2022-282
Preprint. Discussion started: 14 October 2022

during the outbreak of COVID-19 in China. Science of The Total Environment, 764, 142886. DOI: 10.1016/j.scitotenv.2020.142886

Ziemke, J. R., Labow, G. J., Kramarova, N. A., McPeters, R. D., Bhartia, P. K., Oman, L. D., ... & Haffner, D. P. (2021). A global ozone profile climatology for satellite retrieval algorithms based on Aura MLS measurements and the MERRA-2 GMI simulation. Atmospheric Measurement Techniques, 14(10), 6407-6418.